Mitigation of Tokamak Disruptions Using High-Pressure Gas Injection

D. G. Whyte,[1] T. C. Jernigan,[2] D. A. Humphreys,[3] A. W. Hyatt,[3] C. J. Lasnier,[4] P. B. Parks,[3] T. E. Evans,[3] M. N. Rosenbluth,[3] P. L. Taylor,[3] A. G. Kellman,[3] D. S. Gray,[1] E. M. Hollmann,[1] and S. K. Combs[2]

[1]*University of California, San Diego, California*
[2]*Oak Ridge National Laboratory, Oak Ridge, Tennessee*
[3]*General Atomics, San Diego, California*
[4]*Lawrence Livermore National Laboratory, Livermore, California*

(Received 6 March 2002; published 12 July 2002)

High-pressure gas-jet injection of neon and argon is shown to be a simple and robust method to mitigate the deleterious effects of disruptions on the DIII-D tokamak. The gas jet penetrates to the central plasma at its sonic velocity. The deposited species dissipates $> 95\%$ of the plasma by radiation and substantially reduces mechanical stresses on the vessel caused by poloidal halo currents. The gas-jet species-charge distribution can include $> 50\%$ fraction neutral species which inhibits runaway electrons. The favorable scaling of this technique to burning fusion plasmas is discussed.

DOI: 10.1103/PhysRevLett.89.055001 PACS numbers: 52.40.Hf, 52.35.Py, 52.55.Fa

The avoidance and mitigation of disruptions are critical issues in advancing the tokamak concept as a viable energy source using magnetic confinement fusion. A disruption is initiated by a global instability that causes a rapid ($\sim 10^{-3}$ s) thermal quench (TQ) of the plasma thermal energy. The now highly resistive plasma causes he confining poloidal magnetic field to decay during the toroidal current quench (CQ). The disruption causes damage by these means: (i) plasma-conducted thermal loading of wall surfaces during the thermal quench, (ii) $\mathbf{J} \times \mathbf{B}$ forces from vessel poloidal halo currents induced by the current quench, and (iii) the conversion of the toroidal plasma current into relativistic runaway electrons (RE) that eventually are stopped by the wall.

High-pressure gas injection (HiPGI) of moderate-Z noble gases can provide adequate mitigation of disruption-caused damage. HiPGI is demonstrated on the DIII-D tokamak (Fig. 1), using preemptive injection into stable plasmas. A 7 MPa reservoir at room temperature is equipped with a fast-acting valve, releasing $\sim 4 \times 10^{22}$ particles (atoms or molecules) over 2–5 ms into a port adjacent to the DIII-D plasma [1]. Based on the port dimensions (diameter = 0.15 m, length ~ 0.5 m) we estimate the gas-jet neutral density as $n_0 \sim 4 \times 10^{24}$ m^{-3} and ram pressure as $P \sim \rho v^2 \sim 30$ kPa on entering the plasma. A gauge at the valve opening confirms that pressures are the same for the different gases used: D_2, helium, neon, and argon. The injected impurity density distributed in the 20 m^3 plasma volume is $\sim 2 \times 10^{21}$ m^{-3}, about 70 times the electron inventory of the target plasma: $n_e \sim 3 \times 10^{19}$ m^{-3}, $\langle T_e \rangle \sim 1.4$ keV, $\langle P_e \rangle \sim 7$ kPa, $T_{e,\text{central}} \sim 4$ keV.

The gas jet is found to penetrate through the plasma at approximately the sonic speed for all gases injected, delivering to the hot central plasma the large quantity of impurity atoms needed for effective disruption mitigation. A cold front, caused by dilution or radiation from the deposited gas species, is followed through the plasma using several electron temperature diagnostics (Fig. 1), including Thomson scattering, soft x-ray emissions and electron-cyclotron emissions. The jet propagation is consistent both with measured transit velocity of the jet through vacuum and with the expected sound speed (e.g., $c_s \sim 250$ m/s for Ar), but is not highly dependent on the radiation properties of the gas. The various gases follow the expected decrease in sound speed with atomic mass (m), namely, $v_{\text{jet}} \propto m^{-1/2}$. Coincident with the central penetration of the jet, the central n_e increases an order of magnitude due to ionization of the deposited gas, and the central T_e collapses in <0.1 ms, initiating the current quench. The experimental observations are therefore consistent with the jet

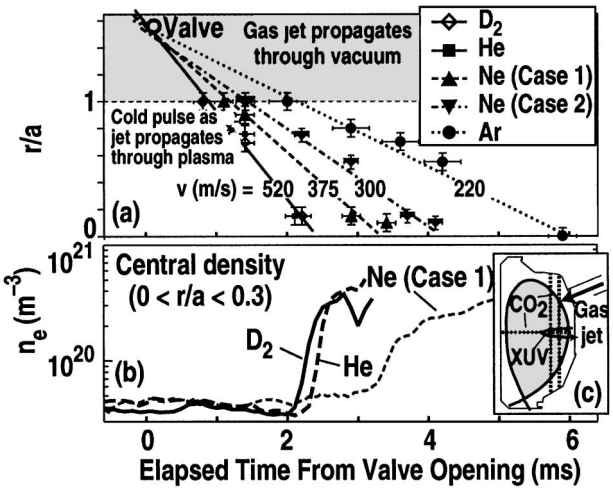

FIG. 1. The high-pressure gas jet penetrates to the core plasma at approximately sonic velocity. (a) Cold pulse (caused by dilution/radiation from jet material and indicated by various plasma temperature diagnostics) propagates through plasma at the same speed as the jet moves through vacuum between valve and edge plasma. (b) Corresponding central electron density rise (Ar data not available) from interferometer inversion. (c) Target plasma shape and diagnostic chords.

penetrating through the plasma as a neutral gas. This is in contrast to the low-pressure gas injection system used for plasma fueling which ionize in the plasma edge [2].

We hypothesize that the gas penetration is due to the high local neutral pressure and density of the jet although a fully developed model on gas-jet penetration is not yet available. We note first that the DIII-D gas jet has passed an important threshold, namely, the local ram pressure of the jet ($\sim$30 kPa) exceeds the volume-averaged plasma electron pressure ($\sim$7 kPa). Therefore, in the hydrodynamic sense it is difficult for the plasma to stop the forward motion of the jet until it reaches the higher-pressure central plasma ($\sim$40 kPa). Furthermore, the large density and size of the jet effectively shield electrons from the center of the jet; that is, the stopping distance for keV electrons is significantly smaller than the diameter of the jet.

The self-consistent time evolution of the impurity ionization state distribution and radiation/energy balance for the injected gas impurity is calculated using the KPRAD (killer pellet radiation) numerical simulation [3]. The simulation uses charge-state-resolved atomic rate coefficients, including charge-state-resolved radiation rates, $L_{\mathrm{rad},Z}$, volume-averaged target plasma parameters, and time-of-flight sonic velocity deposition. The deposited gas impurity rapidly quenches the electron plasma thermal energy through line radiation. The strong electron-ion collisional coupling allows ion energy dissipation. Since the global parallel current density, j (A m^{-2}), cannot change on this time scale (≤ 0.1 ms), the thermal equilibrium of the current quench plasma ($W_{\mathrm{th}} \sim 0$, $dW_{\mathrm{th}}/dt \sim 0$) is determined by the equality of impurity-radiated power, P_{rad} (W m^{-3}) to Ohmic heating, P_{Ohmic} ($= \eta j^2$), namely,

$$P_{\mathrm{rad}} \equiv n_e n_{\mathrm{imp}} \sum_Z L_{\mathrm{rad},Z} = \eta j^2 \propto Z_{\mathrm{eff}} T_e^{-3/2 j 2}, \quad (1)$$

where n_e and n_{imp} (m^{-3}) are the free electron and impurity densities, respectively, $L_{\mathrm{rad},Z}$ (W m^3) is the collisional excitation radiative cooling rate of impurity charge-state Z, and η (Ω m) is Spitzer resistivity. Equation (1) determines T_e and parallel electric field, E_{par} through Ohm's law $E_{\mathrm{par}} = \eta j$. It is important to note that $L_{\mathrm{rad}} \propto \exp(-I/T_e)$ when T_e is well below the ionization potential, I, of the charge state. Therefore T_e and, hence, E_{par} are only logarithmically sensitive to the density of injected impurity and depend most strongly on impurity species. This is demonstrated in Fig. 2 for the case of a singly ionized ($Z_{\mathrm{eff}} = 1 = \langle Z \rangle$, average charge state) species of our candidate noble gases. Note that a nearly tenfold increase in the product of n_e and n_{imp} results in a very small change in T_e and E_{par} given $Z_{\mathrm{eff}} \sim 1$. This is a most important result with regard to the control of runaway electrons, as will be later discussed.

The model predictions of the current quench plasma are verified experimentally for DIII-D gas injection. The core current quench decay time, τ_{CQ}, is calculated from the L_i/R (inductance/resistance) time using a fixed $L_I =$

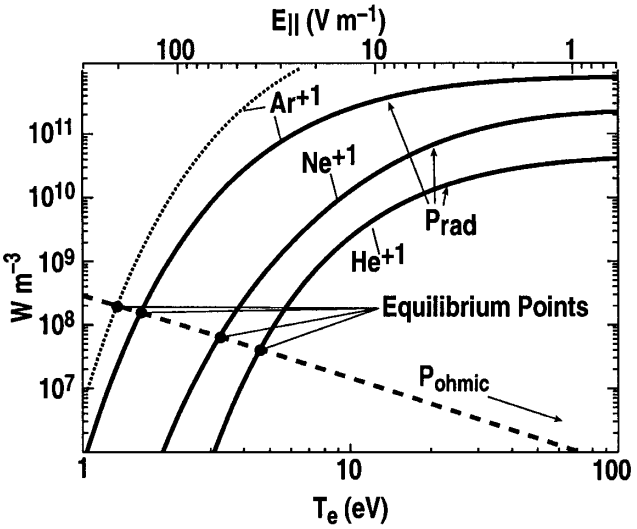

FIG. 2. The current quench T_e and $E_{\|}$ are determined by the crossing of Ohmic and radiated power densities for singly ionized noble gases (Fig. 1). Case shown: $n_{\mathrm{imp}} = n_e = 10^{21}$ m^{-3}, $j = 10^6$ A m^{-2}, $Z_{\mathrm{eff}} = 1$, except the dotted line for Ar^{+1} with $n_{\mathrm{imp}} = n_e = 3 \times 10^{21}$ m^{-3}, indicating the insensitivity of T_e to n_{imp}.

1.5 μH (Table I) and is therefore a test of our calculated parallel electric field, E_{par} ($\tau_{\mathrm{CQ}} \propto 1/E_{\mathrm{par}}$), a critical parameter for runaway electrons. The model follows well the measured magnitude and trend of decreasing τ_{CQ} (increasing E_{par}) with an increasing noble gas atomic number. The absolute agreement is acceptable considering the uncertainty in calculated L_{rad} values and L_I (which assumes the simplest case of uniform current distribution in the plasma). The average charge state of the impurity is measured from particle balance ($\langle Z \rangle = \Delta n_e / n_{\mathrm{imp}}$) and is found to be near or less than unity (Table I), with $\langle Z \rangle$ decreasing with Z_{imp}, also in agreement with the model. Since Spitzer resistivity has been verified experimentally in DIII-D during the current quench [4], the independent confirmations of η and Z_{eff} in Table I also validate the calculated T_e. For example, the He gas-jet injection into an Ohmic plasma [4] measured $T_e \sim 3.8$–5.3 eV, compared to KPRAD calculated average $T_e \sim 4.5$ eV through the current quench.

We further note the good agreement between model and experiment obtained for the injection of argon cryogenic pellets (Table I), another technique used for disruption mitigation. The pellet n_{imp} is only 1% of the gas jet. This results in a plasma with significantly higher $\langle Z \rangle \sim 5$, but one that has higher T_e because radiated power is dominated by this higher charge state. Thus the changes in T_e and Z_{eff} cancel out, resulting in the nearly same resistivity, τ_{CQ} and E_{par}

In unmitigated disruptions during the thermal quench [2], thermal conduction typically caries 20%–40% of the plasma's thermal (W_{th}) and magnetic (W_{mag}) energy to the divertor. The HiPGI of argon or neon provides optimal thermal mitigation with its combination of good impurity penetration, large impurity quantity, and high radiation rates. Divertor tile thermography shows a thermal quench

TABLE I. KPRAD model calculated current quench parameters and RE amplification factors for different disruption mitigation scenarios compared to experimentally measured values of average charge state, $\langle Z \rangle$, from charge balance and L/R current decay time, τ_{CQ} for core plasma. DIII-D target plasma: $\langle T \rangle = 1.5$ keV, $V \sim 18$ m^3, $j = 0.66$ MA m^{-2}, $L = 1.5$ μH.

Mitigation Scenario			Model					Experiment	
Type		n_{imp} (m^{-3})	$\langle Z \rangle$	T_e (eV)	E_{par}/E_c	G	τ_{CQ} (ms)	$\langle Z \rangle$	τ_{CQ} (ms)
Jet	He	2×10^{21}	0.95	3.43	10.4	1.64	4.5	0.8 ± 0.3	5 ± 0.3
Jet	Ne	2×10^{21}	0.94	2.53	3.1	0.61	3.0	0.4 ± 0.15	2.4 ± 0.4
Jet	Ar	2×10^{21}	0.45	1.46	3.81	0.47	1.38	0.3 ± 0.1	1.8 ± 0.1
Pellet	Ar	2×10^{19}	5.9	7.5	312	1.1	2.0	5.7 ± 1	2.1 ± 0.2

temperature rise consistent with deposition of ~3%–5% W_{th}, the fraction expected from uniform radiative dissipation. Indeed, the integrated radiated energy is measured to account for the total plasma energy ($W_{th} + W_{mag}$) within the experimental uncertainties. Using nonreactive, fully recycling noble gases minimizes deterioration of wall and vacuum conditions for subsequent plasma discharges. Pumping systems were undamaged (peak vessel pressure ~10 Pa) and no traces of injected impurity were found in the breakdown of subsequent discharges.

The most severe halo currents are found during vertical displacements events (VDE), where the entire plasma moves vertically into the wall. In DIII-D gas-jet experiments, poloidal vessel halo currents, and their nonaxisymmetric peaking, we reduced about a factor of 2–4 compared to unmitigated VDE cases. An additional benefit is that neon/argon HiPGI causes the core plasma to remain centered vertically in the vacuum vessel until the closed flux surfaces are lost (Fig. 3), meaning that the core current decay rate is much faster than the vertical instability growth rate. This feature further reduces the vessel forces resulting from poloidal halo currents by maintaining a high edge safety factor throughout the current quench [4].

Relativistic runaway electrons (RE) are produced when E_{par}, which accelerates electrons, is greater than the critical electric field, E_c, set by collisional drag, namely, E_c (V/m) $= mc\nu/e \sim 10^{-21} n_{e,T}$. The slowing down rate is given by ν (s^{-1}) $\sim 5.4 \times 10^{-19} n_{e,T}$ for relativistic electrons streaming through background electrons of density $n_{e,T}$ (m^{-3}). The definition of $n_{e,T}$ includes both free, n_e, and bound electrons [5] since both contribute to collisional drag of relativistic electrons. Runaway electrons experience amplification via the knock-on avalanche process in the current quench [6]. The runaway electrons growth rate $\gamma_{RE} \propto \nu(E_{par}/E_c - 1)$. The total runaway electrons' amplification factor through the current quench of duration τ_{CQ} is then approximately e^G, where $G = \gamma_{RE}\tau_{CQ} \propto \gamma_{RE}/E_{par}$. The runaway electrons' amplification gain is calculated from the benchmarked KPRAD disruption model results (E, τ_{CQ}, etc.) and the analytic growth rate formula from Ref. [6] for several mitigation scenarios (Table I, Fig. 4).

A comparison of the argon pellet and gas jet illustrates the effectiveness of HiPGI in controlling RE on DIII-D (Fig. 4). No significant population of runaway electrons is found for neon and argon HiPGI on DIII-D, unlike the pellet which shows a runaway electron current tail > 100 kA in the current quench. The parameter of E_{par}/E_c, critical to producing runaway electrons, is greatly reduced from ~300 in the pellet case to ~3 in the gas-jet case, mostly by providing a large density of bound electrons since $\langle Z \rangle < 1$. This occurs because the accelerating E_{par} is roughly the same in the two cases (matched by the model, Table I) yet the gas jet injects ~100 times the density of impurities as the pellet.

Most importantly, this result points to a means of complete suppression of runaway electrons by forcing $E_{par}/E_c < 1$ ($G < 0$). KPRAD calculations indicate complete suppression occurs with $n_{imp} > 7 \times 10^{21}$ m^{-3} using

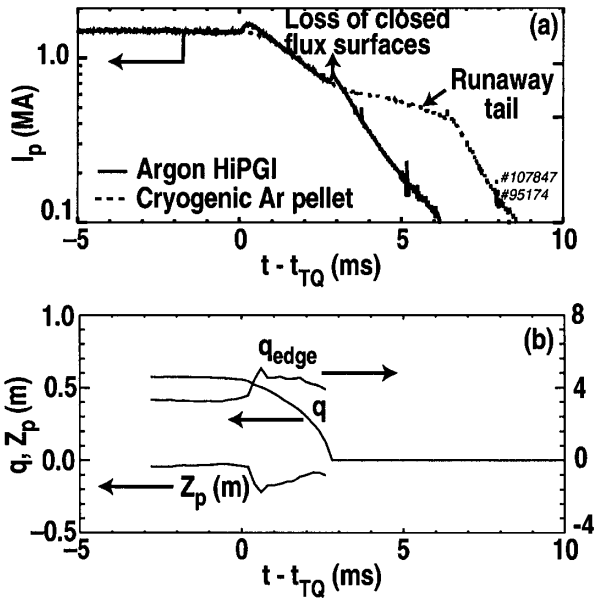

FIG. 3. Time traces of (a) total plasma current, I_p. In comparison to Ar cyrogenic pellet injection, no sign of confined runaway electron current is found for HiPGI. (b) Core plasma centroid position (midplane: $Z_p = 0$) and core plasma minor radius, a, and edge safety factor, q, during argon HiPGI on DIII-D.

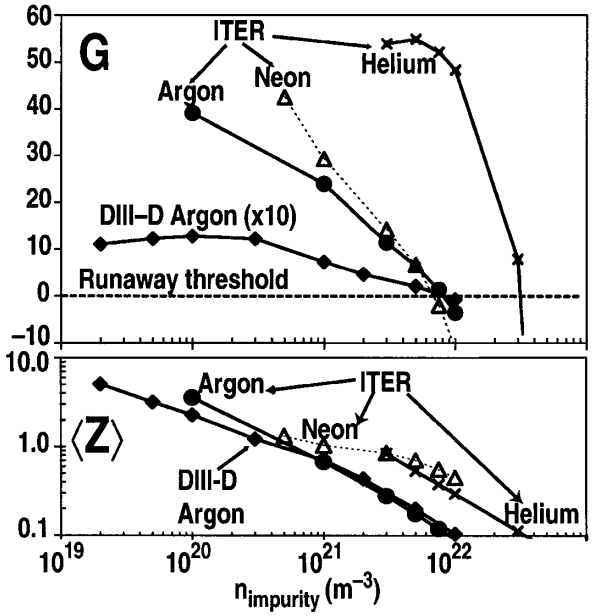

FIG. 4. Calculated surface-averaged runaway electron amplification gain factor (G) and $\langle Z\rangle$ vs $n_{\rm imp}$ for helium, neon, and argon HiPGI into ITER-EDA and DIII-D. ITER-EDA target: $\langle T\rangle = 10.5$ keV, $V = 1890$ m^3, $j = 0.55$ MA m^{-2}, $R, a = 8, 2.8$ m, $L = 13$ μH. DIII-D case as in Table I.

HiPGI of neon or argon on DIII-D (Fig. 4). This is only a factor of 3 larger than our current experimental value, $n_{\rm imp} \sim 2 \times 10^{21}$ m^{-3}. In the model, this result arises primarily from the increasing neutral gas density as $n_{\rm imp}$ is increased and $\langle Z\rangle$ decreases. However, $E_{\rm par}$ is nearly constant as $n_{\rm imp}$ increases, since it is determined primarily by the atomic physics (i.e., cooling rates) of the injected impurity, and Ohmic heating is little affected by neutral species. Therefore, $n_{e,T}$ and E_c can in a sense be ''arbitrarily'' increased by orders of magnitude by the large $n_{\rm imp}$ associated with HiPGI. This trend of nearly constant $E_{\rm par}$ with ever increasing $n_{\rm imp}$ is indeed confirmed by DIII-D data and is expected from our simple current quench model (Table I). Finite transport losses of runaway electrons [7,8] will lower the $n_{\rm imp}$ necessary for suppression. Gas injection is the most reliable technique to raise gas density in the plasma volume during the current quench. Pellets or liquids injected during the current quench simply pass through the plasma since the very cold plasma does not readily evaporate them.

The extrapolation of these results to reactor class plasmas is important because the potential for damage from thermal loads and runaway electrons increases with device size. For convenience the ITER (Final Design Review, 1999, $R = 8$ m, $I_p \sim 20$ MA [9]) tokamak is used as the example reactor for our KPRAD simulations.

On the assumption of sonic-jet penetration, KPRAD simulations calculate that, much like DIII-D, the ITER core plasma is rapidly quenched through radiation by the injection of argon or neon with $n_{\rm imp} \sim 10^{21}$ m^{-3}. If the plasma thermal and magnetic energies are dispersed uniformly through radiation, this does not lead to surface melting/ablation for the wall materials [10]. The rapid quench reduces VDE induced halo currents and vessel forces. The key to jet penetration is that the jet pressure exceeds the plasma pressure. Then, in order for the jet to penetrate to the center of the hotter ($\langle T_e\rangle \sim 10$ keV) and higher pressure ($\langle P_e\rangle \sim 100$ kPa) burning plasma, a modest increase from our DIII-D jet ($P \sim 30$ kPa) seems necessary.

Based on our disruption modeling [Eq. (1)], we expect similar disruption mitigation plasma conditions on DIII-D (Table I) and ITER (Fig. 4). The most important difference is that ITER has a much longer $\tau_{\rm CQ}$, since L/R approximately scales with the cross-sectional area at fixed resistivity, η. For small impurity concentrations ($n_{\rm imp} < 10^{21}$ m^{-3}), KPRAD calculations recover previous results of amplification gain ($\sim e^{50}$) for ITER (Fig. 4) so large that any seed runaway electrons will result in the nearly complete conversion of plasma current into runaway electrons [5]. However, as argon/neon $n_{\rm imp}$ is increased to $\sim 8 \times 10^{21}$ m^{-3}, runaway electrons can be suppressed by forcing Epar/Ec<1\hbox{.} The scaling of the gas injection to the large ITER volume (~ 2000 m^3) is reasonable—a 5-liter reservoir at 100 bar provides the necessary $n_{\rm imp}$. We find the threshold for helium runaway electron suppression is somewhat higher. Therefore argon or neon appear to be ideal candidate gases; they provide thermal mitigation with high radiative rates, and more bound electrons per injected atom to suppress runaway electrons.

This work is supported by the U.S. Department of Energy under Contracts No. DE-AC03-99ER54463, No. DE-AC05-00OR22725, No. W-7405-ENG-48, and Grant No. DE-FG03-95ER54294.

[1] P. L. Taylor *et al.*, Phys. Plasmas **6**, 1872 (1999).
[2] A. W. Hyatt *et al.*, in *Proceedings of the 23rd European Conference on Controlled Fusion and Plasma Physics, Kiev, Ukraine, 1996* (European Physical Society, Innsbruck, 1996), Vol. 20A, p. 287.
[3] D. G. Whyte v, in *Proceedings of the 24th European Conference on Controlled Fusion and Plasma Physics, Berchtesgaden, Germany, 1997* (European Physical Society, Innsbruck, 1997), Vol. 21A, p. 1137.
[4] D. A. Humphreys and D. G. Whyte, Phys. Plasmas **7**, 4057 (2000).
[5] P. B. Parks, M. N. Rosenbluth, and S. V. Putvinski, Phys. Plasmas **6**, 2523 (1999).
[6] M. N. Rosenbluth and S. V. Putvinski, Nucl. Fusion **37**, 1355 (1997).
[7] R. Yoshino, S. Tokudo, and Y. Kawano, Nucl. Fusion **39**, 151 (1999).
[8] R. W. Harvey, V. S. Chan, S. C. Chiu, T. E. Evans, M. N. Rosenbluth, and D. G. Whyte, Phys. Plasmas **7**, 4590 (2000).
[9] S. Mirnov *et al.*, Nucl. Fusion **39**, 2577 (1999).
[10] B. V. Kuteev, V. Yu Sergeev, and S. Sudo, Nucl. Fusion **35**, 1167 (1995).